Applied Catalysis B: Environmental 95 (2010) 383–392

Contents lists available at ScienceDirect

Applied Catalysis B: Environmental

journal homepage: www.elsevier.com/locate/apcatb

Effect of phase structures on the photocatalytic activity of surface fluorinated TiO_2

Kangle Lv [a,b,*], Xiaofang Li [a], Kejian Deng [a,**], Jie Sun [a], Xianghong Li [a], Mei Li [a,b]

[a] Key Laboratory of Catalysis and Materials Science of the State Ethnic Affairs Commission & Ministry of Education, South-Central University for Nationalities, Wuhan 430074, PR China
[b] State Key Laboratory of Advanced Technology for Materials Synthesis and Processing, Wuhan University of Technology, Wuhan 430070, PR China

ARTICLE INFO

Article history:
Received 2 October 2009
Received in revised form 27 December 2009
Accepted 20 January 2010
Available online 25 January 2010

Keywords:
Photocatalytic degradation
Titanium dioxide
Fluoride
Adsorption
Crystalline phase

ABSTRACT

Nanocrystalline TiO_2 with different contents of anatase were tailored by hydrothermal treatment of the mixed solution of $Ti(SO_4)_2$ and $TiCl_4$ at 250 °C for 24 h, and then calcined at 500 °C for 3 h. The catalysts were characterized by X-ray diffraction, transmission electron microscopy, nitrogen sorption, X-ray photoelectron spectroscopy and UV–vis diffuse reflectance spectra. The as-prepared TiO_2 samples with different contents of anatase have similar BET specific surface areas (30–40 m^2/g) and crystalline sizes (30–40 nm). The effect of surface fluorination on the adsorption and photocatalytic activity of TiO_2 samples was evaluated using Brilliant Red X3B, an anionic azo dye, as the target organic molecule at pH 3.0. Both on anatase and rutile TiO_2, the dark adsorption of X3B was greatly decreased in the presence of fluoride, ascribed to competitive adsorption of fluoride that reduces the positive charges on the catalyst surface. After surface fluorinated by 1.0 mmol/L NaF, the photocatalytic activity of anatase was enhanced by a factor of 2.63. However, 81.3% of the photocatalytic activity was reduced for rutile TiO_2 after surface fluorinated under the same condition. Only when the content of anatase is higher than 40%, can fluoride shows positive effect on the photocatalytic activity of TiO_2. Two reaction models were put forward, based on the photocurrent response, degradation kinetics, hydroxyl radicals quenching and detecting, to illustrate the different effects of fluoride on the photocatalytic degradation of X3B in anatase and rutile TiO_2 suspensions.

1. Introduction

In recent years, in order to solve the increasingly serious environmental pollution problems, heterogeneous semiconductor photocatalysis gradually becomes a popular technique for its potential to control aqueous contaminates or air pollutants [1–3]. Among which, TiO_2 photocatalysis has attracted increasing attention due to its biological and chemical inertness, strong photo oxidization power, cost effectiveness, and long-term stability against photo and chemical corrosion [4–7]. However, a vital problem, i.e., low quantum efficiency (~4%), hampers its widespread practical applications. Therefore, the photocatalytic activity of TiO_2 needs to be further improved [7–11].

It is often observed that efficiency of organic degradation is a function of physical parameters of TiO_2, such as the crystalline phase, crystallinity, particle size, surface area, and so on [8,12]. Recently, several studies have shown that addition of NaF into the aqueous dispersions of TiO_2 can result in significant enhancement in the rate of organic photocatalytic degradation with the preferred solution pH of 3 [4,12–21]. Minero and co-worker ascribed this to the enhanced generation of free $^{\bullet}OH$ radicals in solution, since fluoride displacement of surface OH^- groups forces the valence holes to oxidize solvent water (Eqs. (1) and (2)) [13,14]. This enhanced production of $^{\bullet}OH$ radicals due to NaF addition was confirmed latter by Mrowetz and Selli, using a DMPO-spin trap ESR technique [17]. Interestingly, Choi and co-worker have demonstrated that the surface fluorination of TiO_2 also result in the enhanced photocatalytic degradation of stearic acid [22] and acetaldehyde [23] in gaseous phase, and they ascribed this to the enhanced generation of airborne free $^{\bullet}OH$ radicals.

$$\equiv\text{Ti-OH} + F^- \rightarrow \equiv\text{Ti-F} + OH^- \quad pK_{a1} = 6.3 \tag{1}$$

$$\equiv\text{Ti-F} + H_2O + h_{vb}^+ \rightarrow \equiv\text{Ti-F} + {}^{\bullet}OH_{free} + H^+ \tag{2}$$

$$\equiv\text{Ti-F} + h_{vb}^+ + {}^3O_2 + e^- \rightarrow \equiv\text{Ti-F} + {}^1O_2 \tag{3}$$

Although the majority view is the production of free $^{\bullet}OH$ radicals due to the fluoride replacement of surface hydroxyl groups (Eq. (2)), The relevant mechanism involving surface fluorination and photocatalytic reactions is still remains unclear to some extent [7,12–14,20,22]. Choi et al. [12] found that the photocurrents collected in TiO_2 suspensions and short-circuit photocurrents

* Corresponding author at: Key Laboratory of Catalysis and Materials Science of the State Ethnic Affairs Commission & Ministry of Education, South-Central University for Nationalities, Wuhan 430074, PR China. Tel.: +86 27 67843930; fax: +86 27 67842752.
** Corresponding author. Tel.: +86 27 67843930; fax: +86 27 67842752.
E-mail addresses: lvkangle@mail.scuec.edu.cn (K. Lv), Dengkj@scuec.edu.cn (K. Deng).

0926-3373/$ – see front matter © 2010 Elsevier B.V. All rights reserved.
doi:10.1016/j.apcatb.2010.01.017

generated on an illuminated TiO_2/Ti electrode were markedly reduced in the presence of F^-. Therefore, the surface ≡Ti-F group was considered as an electron-trapping site, which results in the reduction of the interfacial electron transfer rates by tightly holding trapped electrons due to the strong electronegativity of the fluorine. However, Leng et al. [7] attributed the enhanced photoelectrochemical performance and photocatalytic activity of the fluorinated TiO_2 to the negative-shifted appearing energy band edges, decreased surface recombination centers, and/or favorable charge transfer rate. Pelizzett et al. [24] ascribed the sustained production of H_2O_2, resulted from the reduction of the adsorbed O_2 by photo-generated e_{CB}, on irradiated fluorinated TiO_2 systems to the competition of the fluoride with superoxide/peroxide species for the surface sites of TiO_2, which inhibited the degradation of H_2O_2 in fluorinated TiO_2. Macyk et al. [15] found that the singlet oxygen ($^1O_2$) photogeneration at surface modified TiO_2 by fluoride, which is responsible for the cyanuric acid oxidation (Eq. (3)).

However, the effect of TiO_2 phase structure (especially for the mixed phase of anatase and rutile), on the fluoride effection has not been systematically studied yet. Since the photocatalytic activity of TiO_2 is the complex function of physical parameters of photocatalyst, such as the crystalline phase, crystallinity, particle size, surface area, and so on, the effects of BET surface area and relative crystallinity of the photocatalysts on fluoride effection need to be eliminated.

Now much attention has been paid on the controllable synthesis processes of crystalline TiO_2 [1,25]. Luo et al. [26] synthesized bicrystalline (anatase and rutile) and tricrystalline (anatase, rutile, and brookite) mesostructured titania using triblock copolymer as structure-directing agent and $TiCl_4$ as precursor by varying the solvent and cosolvent. Wu et al. [27] successfully synthesized rutile and anatase with the microemulsion-mediated hydrothermal method by controlling the concentration of HNO_3, which exhibited a possibility of stepwise adjustment of the percentage of anatase and/or rutile phase in the titania product. Zhang et al. [1] successfully synthesized TiO_2 with controllable crystalline and high surface area by simply varying the proportion of $Ti(SO_4)_2$ and $TiCl_4$ in the aqueous phase of microemulsion. However, all of the synthetic methods mentioned above need the use of organic solvent or surfactant, which is harmful to the environment.

In this work, TiO_2 samples with different contents of anatase, and similar BET surface areas and crystalline sizes, were synthesized through hydrothermal method by controlling the proportion of $Ti(SO_4)_2$ and $TiCl_4$. The effect of surface fluorination on the adsorption and photocatalytic activity of the TiO_2 samples with different anatase contents were studied at pH 3.0, using X3B (Fig. 1), an anionic dye, as the target organic pollutant.

2. Experimental

2.1. Preparation of the catalysts

The synthetic TiO_2 samples were prepared by hydrothermal treatment of the mixed solution of $Ti(SO_4)_2$ (1.0 mol/L) and $TiCl_4$ (1.0 mol/L) at various volume ratio. For example, 2.5 mL of $Ti(SO_4)_2$ and 47.5 mL of $TiCl_4$ were mixed, and then dropwise added to 30.0 mL of NaOH (1.5 mol/L) solution under magnetic stirring. The resulted white sol was transferred to a 100-mL of Teflon-lined autoclave. Note the molar percentage of SO_4^{2-} in total anionic concentration was 2.56% ($n_{SO_4^{2-}}/(n_{SO_4^{2-}} + nCl^-)$) in the mixed solution. The autoclave was sealed and kept at 250 °C for 24 h. After being cooled to room temperature, the white precipitates were filtrated through a membrane filter (pore size 0.45 μm), and thoroughly rinsed with distilled water until no SO_4^{2-} and Cl^- in the filtrate were detected by $BaCl_2$ and $AgNO_3$, respectively. Finally, the white cake was calcined at 500 °C for 3 h to obtain the final photocatalyst. A serials of TiO_2 samples with different molar percentage of SO_4^{2-} were also prepared accordingly by adjusting the volume ratio of $Ti(SO_4)_2$ to $TiCl_4$.

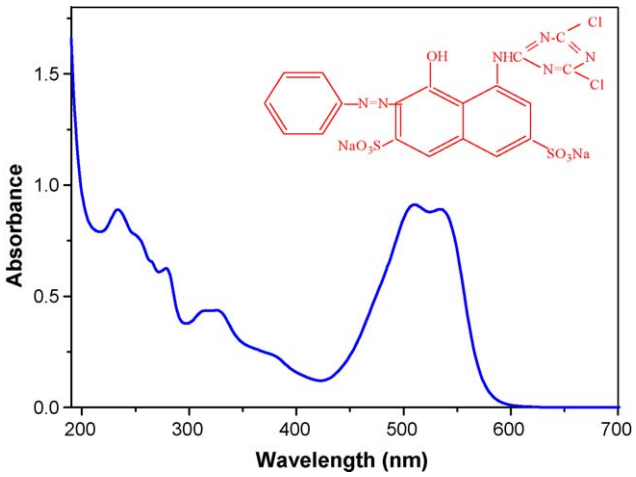

Fig. 1. Structure and electronic absorption spectrum of X3B in water.

2.2. Characterization

The X-ray diffraction (XRD) patterns obtained on a D8- advance X-ray diffractometer (German Bruker) using Cu K*a* radiation at a scan rate of 0.02° s^{-1} were used to determine the crystalline size and identity. The accelerated voltage and applied current were 200 kV and 20 mA, respectively. The average crystalline size of the catalyst was determined according to the Scherrer equation using full-width at half-maximum data after correcting for the instrumental broadening [9,28]. The BET surface areas of the powders were analyzed by nitrogen adsorption in a Micromeritics ASAP 2020 nitrogen-adsorption apparatus (USA). The BET surface area was determined by multipoint BET method using the adsorption data in the relative pressure (P/P_0) range of 0.05–0.3. Pore volume was determined by nitrogen adsorption volume at the relative pressure of 0.994. All the samples were degassed at 180 °C prior to the nitrogen-adsorption measurements. The morphologies of TiO_2 powders were observed on transmission electron microscopy (TEM, Tecnai G20, USA) at an acceleration voltage of 200 kV. X-ray photoelectron spectroscopy (XPS) measurements were performed with a Multilab 2000 XPS system with a monochromatic Mg K*a* source and a charge neutralizer. All of the binding energies were referenced to the C 1s peak at 284.4 eV of the surface adventitious carbon. UV–vis absorbance spectra of as-prepared TiO_2 particles were obtained for the dry-pressed disk samples with a UV–vis spectrophotometer (UV-2550, Shimadzu, Japan). $BaSO_4$ was used as an absorption standard in the UV–vis absorbance experiment. Photocurrent measurements were carried out on an Electrochemical Station (CHI660, China). A collimated light beam from a 300W PLS-SXE-300 xenon lamp was used for excitation of the ITO/TiO_2 electrode. These measurements were carried out with a standard three-electrode assembly. The ITO/TiO_2 electrode, Pt plate, and Ag/AgCl electrode were used as the working, counter, and reference electrodes, respectively. The ITO/TiO_2 electrode was prepared using the as-prepared TiO_2 sample as TiO_2 precursors via the doctor-blade method [29]. KOH (1.0 mol/L) is used as the electrolyte and is saturated with air.

2.3. Adsorption

Reactive Brilliant Red X3B (X3B, Fig. 1), an anionic organic dye, was used as the target organic pollutant. The adsorption isotherm

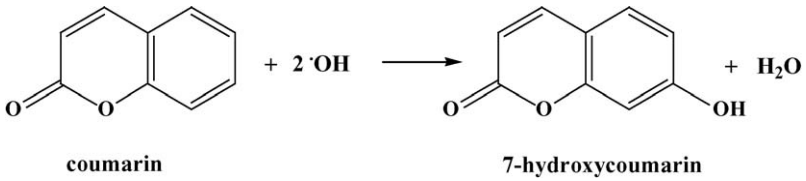

Scheme 1. Formation of 7-hydroxycoumarin in the reaction of coumarin with hydroxyl radicals.

of substrate (X3B and NaF) on TiO_2 was measured in the dark by mixing 50.0 mg TiO_2 with 50.0 mL aqueous solution at pH 3.0 at various initial concentration of substrate C_0. The suspension was first sonicated for 5 min, and then was shaken at a constant rate overnight. After the suspension was filtered through a membrane filter (pore size 0.45 μm), the filtrate was analyzed to get the equilibrium concentration C_2^b. The wavelength for analysis of X3B was 510 nm, whereas the concentration of fluoride was measured by ion-selective electrode on a pHS-3C pH meter [20]. The amount of adsorption, n_2^s, was calculated by the decreased concentration of $(C_0 - C_2^b)$ divided by the amount of catalyst used, and expressed in unit of moles per gram of TiO_2 [19].

2.4. Photocatalytic degradation

The light source (375 W, Shanghai Yamin) emitted mainly at 365 nm, and placed outside a Pyrex-glass reactor at a fixed distance (ca. 10 cm) [19]. During the photocatalytic reaction, the reactor was maintained at room temperature through a water recycle system, and was mechanically stirred at a constant rate. The concentration of TiO_2 was 1.0 g/L, and the initial concentration of X3B was 1.0×10^{-4} mol/L. If necessary, NaF (1.0 mM) was added into the suspension, followed by mechanic shaking in the dark overnight, and the solution pH was adjusted to 3.0 by diluted NaOH and $HClO_4$. Note that ClO_4^- is a weakly adsorbed anion, which shows a negligible influence on the photocatalytic degradation [13]. Before irradiation, the reaction mixture containing necessary components was sonicated first for 5 min, and then was shaken overnight in the dark. At given intervals of irradiation, small aliquots were withdrawn by a syringe, and filtered through a membrane (pore size 0.45 μm). The concentration of X3B remaining in the filtrate was then analyzed by an Agilent 8451 spectrometer.

2.5. Determination of free •OH radicals

The analysis of the formation of free •OH radicals, produced in suspensions of surface fluorinated TiO_2 under UV irradiation (Eq. (2)), was performed by photolumenscence (PL) technique using coumarin as a probe molecule, which readily reacted with •OH radicals to produce highly fluorescent product, 7-hydroxycoumarin (Scheme 1) [30,31]. The suspensions of TiO_2 (1.0 g/L, pH 3.0) containing coumarin (0.5 mmol/L) and NaF (1.0 mmol/L) is mixed under magnetic stirring, and then was shaken overnight and irradiated as that of the photocatalytic experimental section (Section 2.4). Sampling was performed in every 2 min and the filtrate was analyzed on a Hitachi F-7000 fluorescence spectrophotometer with the excitation wavelength of 332 nm.

3. Results and discussion

3.1. Preparation of controllable crystalline titania

XRD was usually used for identification of the crystal phase and to estimate the anatase-to-rutile ratio as well as the crystallite size of each present phases. The XRD peaks at around $2\theta = 25.25^\circ$ (1 0 1) in the spectrum of TiO_2 are identified as the anatase form, whereas the XRD peaks at $2\theta = 27.42^\circ$ (1 1 0) are taken as the rutile form [28]. Fig. 2 lists some of the TiO_2 samples prepared with different molar percentage of SO_4^{2-}. The content of anatase can be calculated from the integrated intensities of the anatase (1 0 1) and rutile (1 1 0) peaks according to the following equation [6,28,32]:

$$W_A = \frac{0.886 I_A}{0.886 I_A + I_R} \quad (4)$$

where I_A and I_R represent the integrated intensity of the anatase (1 0 1) and rutile (1 1 0) peaks, respectively. For simplification, TiO_2 samples in Fig. 2 were denoted as AT*x*, where *x* is the anatase content (%). For example, the content of anatase for TiO_2 sample prepared from 2.56% of SO_4^{2-} is calculated to be 7.6% (Fig. 2b). Therefore, it is denoted as AT7.6.

It is found that pure rutile (AT0, Fig. 2a) and pure anatase (AT100, Fig. 2i), were obtained when the molar percentage of SO_4^{2-} were 0 and 100, respectively. Other samples were the mixed phases of anatase and rutile prepared by varying the molar percentage of SO_4^{2-} (Fig. 2b–h). The relationship between the molar percentage of SO_4^{2-} and the content of anatase in TiO_2 powder presents an S-shaped curve (Fig. 3). A linear relationship between anatase content and concentration of SO_4^{2-} is found when the molar percentage of SO_4^{2-} is from 2.56% to 3.09% (inset of Fig. 3), which is similar to the report of Zhang [1]. When the molar percentage of SO_4^{2-} is less than 2.04% in the preparation procedure, only the rutile phase was obtained. Pure anatase can be observed in the TiO_2 powder when the molar percentage of SO_4^{2-} is greater than 3.90%. That is to say, TiO_2 samples with different content of the anatase can be effectively controlled by simply varying the proportion of $Ti(SO_4)_2$ and $TiCl_4$ in the mixed solution before autoclaved.

It has been reported that the presence of SO_4^{2-} accelerated the growth of anatase TiO_2 clusters, which could be ascribed to the steric effect of SO_4^{2-} during the polycondensation of TiO_6^{2-} octahedral hydroxyls [1]. On the other hand, there is a weak steric

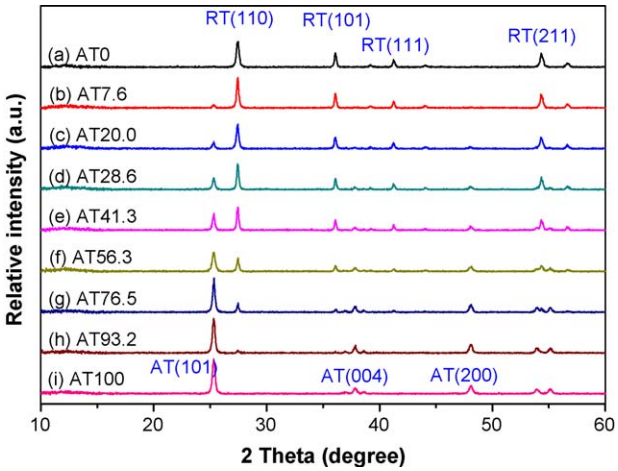

Fig. 2. XRD patterns of the prepared TiO_2 samples. The corresponding mole percents of sulfate are (a) 0, (b) 2.56, (c) 2.67, (d) 2.77, (e) 2.83, (f) 2.93, (g) 3.04, (h) 3.09 and (i) 100, respectively.

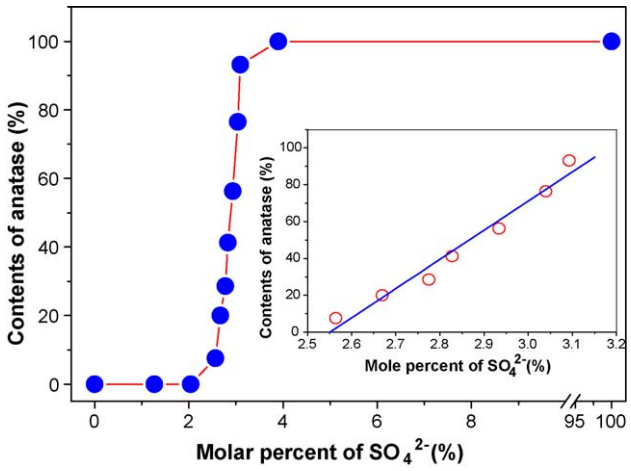

Fig. 3. Relationship between the contents of anatase and the molar percent of SO_4^{2-} (inset: the linear fit of samples with the mole percentage of SO_4^{2-} from 2.56 to 3.09).

effect for Cl^- because of its small radius. Meanwhile, the addition of Cl^- generally favors the formation of rutile crystallites [33,34]. As a result, different rutile/anatase mixtures can be prepared by changing the proportions of SO_4^{2-} and Cl^- in the aqueous phase.

The average crystalline sizes, BET surface areas and pore volumes of TiO_2 samples in Fig. 2 are listed in Table 1. It can be seen that these TiO_2 samples possess similar BET surface areas (30–40 m^2/g) and average crystalline sizes (30–40 nm).

3.2. Morphology of the photocatalyst

Distinctly different crystal morphologies have been observed for the pure anatase and rutile TiO_2 powders (Fig. 4). The anatase crystallites (AT100) assume rounded shapes and have typical sizes of 30–40 nm (Fig. 4e), which is consistent with the result detected by XRD (Fig. 2 and Table 1). However, rutile crystallizes as nanorods with diameters of ca. 40 nm and lengths of up to 300–400 nm (Fig. 4a). High-resolution TEM analysis (Fig. 4b and f) reveals the highly crystalline features of the TiO_2 samples. The fringes with a lattice spacing of 0.35 and 0.23 nm correspond to the anatase (1 0 1) and rutile (2 0 0) crystallographic planes of TiO_2 nanoparticles, respectively. With increasing the molar percentage of SO_4^{2-}, The content of anatase increases and the morphology of TiO_2 sample changes from nanorod to rounded nanoparticles. For example, Fig. 4c shows a mixed phase TiO_2 sample of AT41.3 prepared from the SO_4^{2-} molar percentage of 2.83.

3.3. XPS analysis

To reveal the role of sulfate species in the preparation and crystallization of TiO_2, XPS spectra of the samples were measured. Fig. 5 shows the XPS survey spectra of AT0 and AT100, respectively. It can be seen that AT0 only contains Ti, O and C elements, with sharp photoelectron peaks appearing at binding energies of 459 (Ti 2p), 530 (O 1s) and 285 eV (C 1s), respectively [28,35]. The carbon peak is attributed to the residual carbon from the sample and adventitious hydrocarbon from XPS instrument itself. However, the sample of AT100 not only contains Ti, O and C, but also a small amount of S atom (0.8 at.%). High-resolution XPS spectrum of the S 2p region further confirms the presence of sulfur (inset of Fig. 5). The peak of S 2p with a binding energy of 169.0 eV can be attributed to the S (+VI) [28,35,36], which is assigned to the SO_4^{2-} ions adsorbed on the surface of TiO_2 powders [35,37].

3.4. UV–vis diffuse reflectance spectra

The UV–vis diffuse reflectance spectra (DRS) of the obtained TiO_2 samples were measured as shown in Fig. 6. Compared with AT100, the sharp decrease in DRS of AT0 is red-shifted for about 25 nm (390 nm for AT100 and 415 nm for AT0, respectively). The optical band gaps, judging from the onset of the DRS, were estimated to be about 3.2 and 3.0 eV for AT100 and AT0, respectively. The values are in accord with the reported values for anatase and rutile TiO_2 [1,10].

3.5. Photocurrent test

Usually, the value of photocurrent indirectly reflects the semiconductor's ability of generating and transferring of photo-generated charge carriers under irradiation [12,29]. Fig. 7 shows the photocurrent response of three TiO_2 samples (AT0, AT100 and p25) coated on ITO electrodes in a photoelectrochemical cell in several on–off cycles. A prompt generation of photocurrents are observed and with good reproducibility when the ITO/TiO_2 electrodes are illuminated with a 300W PLS-SXE-300 xenon lamp. While the PLS-SXE-300 xenon lamp is off, the value of photocurrent for all the ITO/TiO_2 samples are instantaneously close to zero. It can be clearly seen that p25 shows the highest photocurrent value (about 0.5 mA cm^{-2}) among the three TiO_2 samples, and the photocurrent value for AT100 (about 0.3 mA cm^{-2}) is much higher than that of AT0 (about 0.03 mA cm^{-2}). The photocatalytic activity of TiO_2 is highly related to the number of the separated photo-generated charge carriers. Therefore, it can be deduced that the photocatalytic activity of AT100 and p25 is higher than that of AT0.

3.6. Effect of fluoride on the adsorption of X3B

It is known that metal oxide particles suspended in water behave similar to diprotic acids. For TiO_2, hydroxyl groups undergo the following two acid–base equilibria (Eqs. (5) and (6)) [19,38]:

$$\equiv\text{Ti-OH}_2^+ \rightarrow \equiv\text{Ti-OH} + \text{H}^+ \quad \text{p}K_{a5} = 3.9 \tag{5}$$

$$\equiv\text{Ti-OH} \rightarrow \equiv\text{Ti-O}^- + \text{H}^+ \quad \text{p}K_{a6} = 8.7 \tag{6}$$

The point of zero charge (pzc) of p25 TiO_2 (pH_{pzc}) is 6.3. Therefore, in acidic solution, the surface of TiO_2 is positively charged, which facilitates the adsorption of the anionic dye of X3B.

Table 1
Physical properties of the as-prepared TiO_2 samples with different molar percent of SO_4^{2-}.

Sample	Mole percent of SO_4^{2-} (%)	Anatase content (%)	BET surface area (m^2/g)	Pore volume (cm^3/g)	Crystalline size of anatase (nm)	Crystalline size of rutile (nm)
AT0	0	0	30.1	0.43	–	30.8
AT7.6	2.56	7.6	31.2	0.43	–	38.1
AT20.0	2.67	20.0	33.6	0.42	40.0	30.8
AT28.6	2.77	28.6	30.7	0.35	33.3	40.0
AT41.3	2.83	41.3	30.8	0.29	38.1	39.1
AT56.3	2.93	56.3	38.0	0.30	30.7	33.3
AT76.5	3.04	76.5	30.9	0.20	34.8	40.0
AT93.2	3.09	93.2	34.0	0.20	31.6	–
AT100	100	100	35.5	0.21	30.7	–

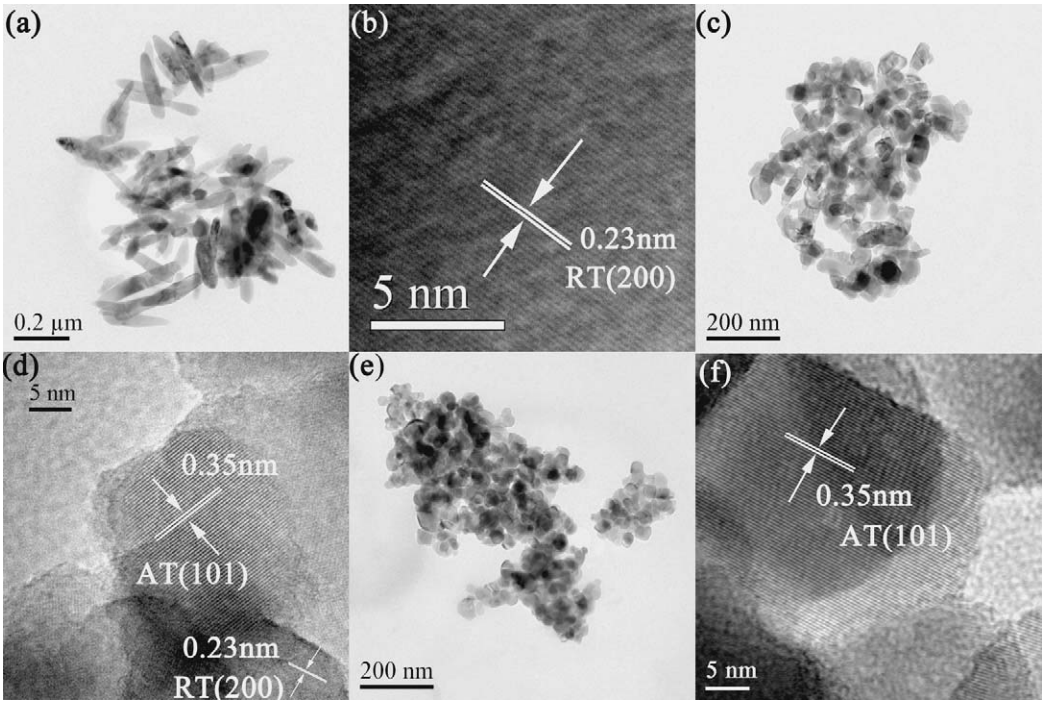

Fig. 4. TEM and HRTEM images of AT0 (a and b), AT41.3 (c and d) and AT100 (e and f) TiO_2 samples.

The adsorption isotherms of X3B at pH 3.0 are shown in Fig. 8a. Since all the adsorption isotherms display the Langmuir-type, the Langmuir equation, $n_2^s/n^s = KC_2^b/(1 + KC_2^b)$, is applied, where n_2^s is the amount of X3B adsorption at C_2^b, the equilibrium concentration of X3B in the bulk solution, n^s is the maximum amount of adsorption, and K is the adsorption constant [39,40]. The resulting adsorption parameters both increase with increasing the contents of anatase (Table 2). It means that anatase TiO_2 shows higher adsorptive ability than rutile TiO_2. The adsorption isotherms of X3B give $n^s = 2.07 \times 10^{-5}$ mol/g, and $K = 4.51 \times 10^4\ M^{-1}$ in rutile TiO_2 (AT0), while $n^s = 3.96 \times 10^{-5}$ mol/g and $K = 6.67 \times 10^4\ M^{-1}$ in anatase TiO_2 (AT100) are obtained.

Different from X3B, the adsorption of fluoride on TiO_2 is a ligand exchange between F^- and ≡Ti-OH on the surface (Eq. (1)). Such complexation is more favorable in an acidic medium, with an equilibrium constant of $10^{7.8}$ (Eq. (7)) [19]:

$$\equiv Ti\text{-}OH_2^+ + F^- \rightarrow \equiv Ti\text{-}F + H_2O \quad pK_{a7} = 7.8 \qquad (7)$$

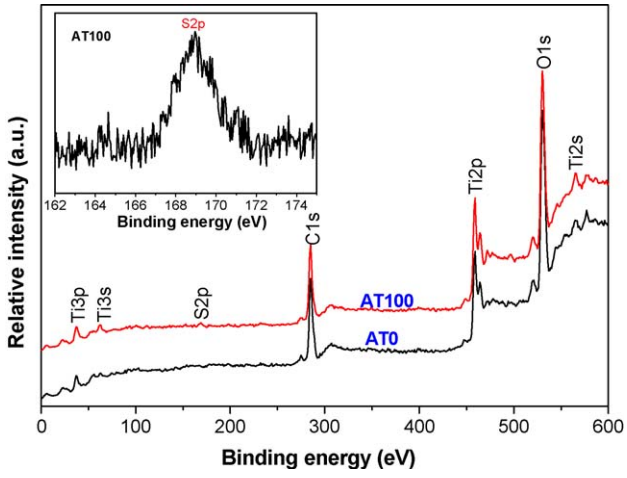

Fig. 5. XPS survey spectra of the TiO_2 powders of AT0 and AT100. Inset is the high-resolution XPS spectrum of the S 2p region of AT100.

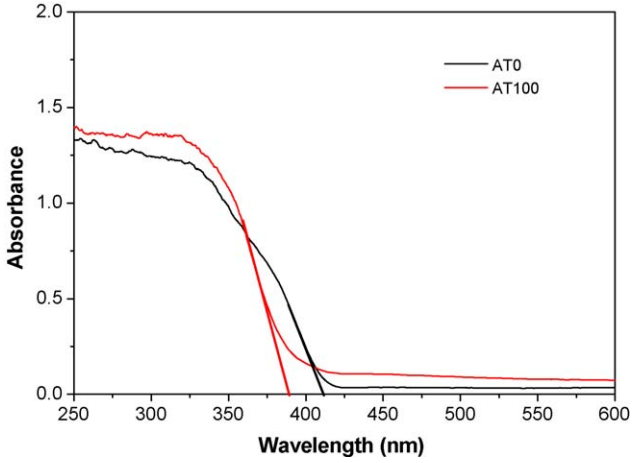

Fig. 6. UV–vis diffuse reflectance spectra of TiO_2 powders (AT0 and AT100).

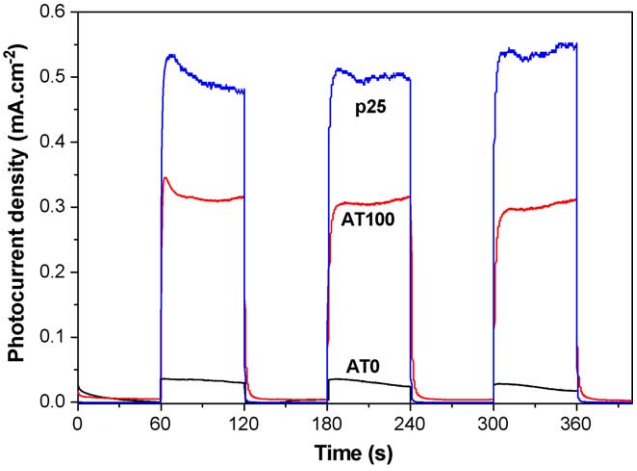

Fig. 7. Photocurrent response of the TiO_2 powders of AT0, AT100 and p25.

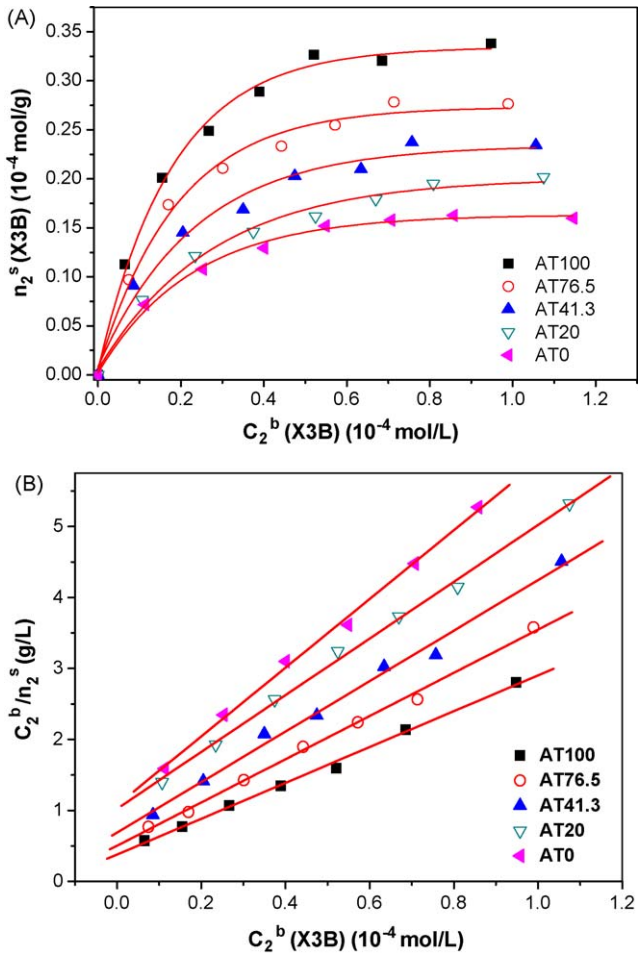

Fig. 8. Adsorption isotherms (A) and the corresponding Langmuir plots (B) of X3B on TiO_2 samples with different contents of anatase from aqueous solution (pH 3.0) at 25 °C.

Table 2
Adsorption parameters of X3B and fluoride on the surface of TiO_2 at pH 3.0.

TiO_2 samples	X3B		Fluoride	
	n^s ($\times 10^{-5}$ mol/g)	K ($\times 10^4$ M^{-1})	n^s ($\times 10^{-4}$ mol/g)	K ($\times 10^4$ M^{-1})
AT0	2.07	4.51	0.91	3.58
AT7.6	2.25	3.78	0.98	2.86
AT20.0	2.50	3.90	0.95	2.65
AT28.6	2.61	4.55	0.98	2.35
AT41.3	2.81	5.18	1.03	2.64
AT56.3	3.01	5.58	1.00	2.87
AT76.5	3.28	6.06	0.97	2.08
AT93.2	3.86	6.35	0.99	2.58
AT100	3.96	6.67	1.09	1.95

The surface specification modeling shows that ≡Ti-F is the dominant species on the surface of TiO_2 at pH 3.0 [13]. Fig. 9 shows the adsorption isotherms of fluoride on TiO_2 samples with different contents of anatase, which also displays the Langmuir-type. Different from X3B, fluoride shows similar adsorption on anatase and rutile TiO_2 (Fig. 9 and Table 2). The maximum amount of adsorption of fluoride on all of the TiO_2 samples is ca. 0.10 mmol/g. Note that the data is smaller than that detected on p25 TiO_2 (0.27 mmol/g) [19], probably due to the different synthetic procedures of TiO_2.

Fig. 10 shows the effect of fluoride on the adsorption of X3B before irradiation. It can be seen that: (1) the adsorption of X3B increases with increasing the contents of anatase, whatever in the absence or presence of fluoride, and (2) the adsorption of X3B is severely retarded in the presence of fluoride. The positive charge of TiO_2 is reduced after the surface is occupied by fluoride (Eq. (5)), which results in a decrease in the adsorption of X3B on fluorinated TiO_2. Since the adsorption of X3B decreases in fluoride modified TiO_2, direct hole oxidation is not favorable for the degradation of X3B in fluorinated TiO_2 suspensions [13,19].

3.7. Photocatalytic degradation of X3B

To study the influence of crystallite phase of TiO_2 on fluoride effection, photocatalytic activity of TiO_2 with different anatase contents in the absence and presence of NaF are evaluated, using X3B as the target organic pollutant. From Fig. 11A, it can be seen that X3B are almost completely photodegraded within 90 and 150 min in naked anatase and rutile TiO_2, respectively. After surface fluorination, the degradation of X3B is greatly enhanced in anatase TiO_2. However, it is severely retarded in rutile TiO_2 after surface fluorination under the same condition (Fig. 11B). The kinetic data for the degradation of X3B can be well fitted by the apparent first-order rate equation, $\ln(C/C_0) = k_{app}t$, where k_{app} is rate constant, C and C_0 are the concentration of X3B at irradiation time $t = 0$ and t, respectively. Fig. 12 shows the effect of fluoride on the degradation rate constant of X3B in TiO_2 with different content of anatase. From Fig. 12A, it can be clearly seen that the

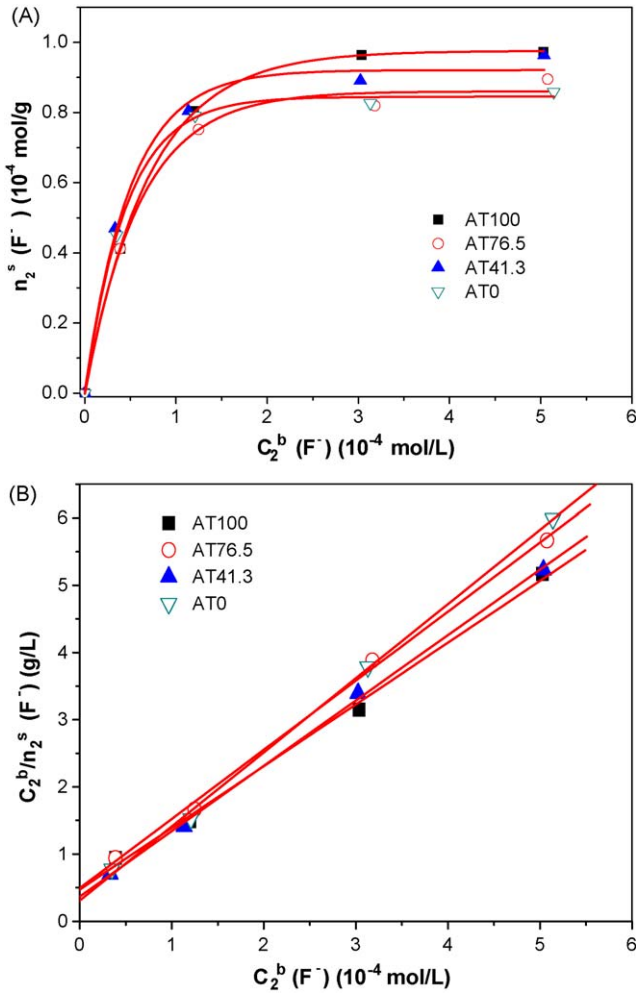

Fig. 9. Adsorption isotherm (A) and the corresponding Langmuir plots (B) of fluoride ions on TiO_2 samples with different contents of anatase from aqueous solution (pH 3.0) at 25 °C.

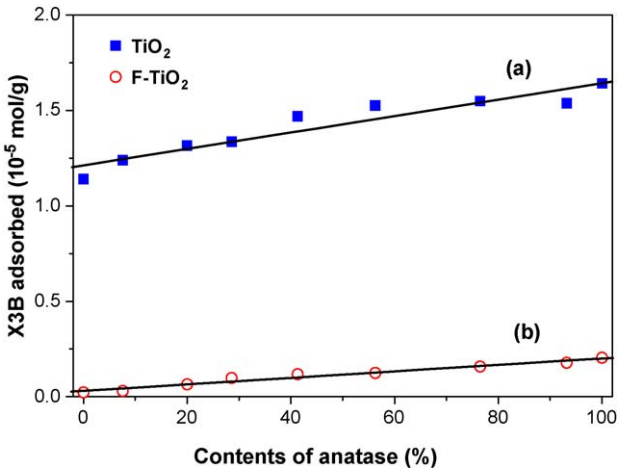

Fig. 10. Amount of X3B adsorbed on the surface of TiO_2 with different contents of anatase in the absence (a) and presence (b) of 1.0 mM fluoride at pH 3.0. The initial concentration of X3B is 1.0×10^{-4} mol/L and the concentration of TiO_2 is 1.0 g/L.

photocatalytic activity of naked TiO_2 samples slightly increases with increasing the contents of anatase. However, fluoride ions play different roles on the photocatalytic activity of anatase and rutile TiO_2. Upon the addition of NaF, the degradation rate of X3B is only increased with anatase, but it is decreased with rutile under similar conditions. The degradation of X3B is enhanced by a factor of 2.63 on AT100 (0.027 and 0.073 min^{-1} in the absence and presence of NaF). However, detrimental effect of fluoride on the photocatalytic activity of rutile is observed, with 81.3% of the photocatalytic activity being decreased for rutile AT0 (rate constant decreases from 0.015 to 0.0028 min^{-1} after surface fluorination). The photocatalytic activity of commercial p25 TiO_2, composed of 80% anatase and 20% rutile, increases by a factor of 1.52 after surface fluorination (rate constant increases from 0.06138 to 0.09343 min^{-1}). For simplification, the ratios of the observed rate constants in the presence and absence of fluoride, $R = K_F/K_0$, are used to denote the degree of photocatalytic degradation rate enhancement due to the addition of NaF. Fig. 12B shows the dependence of the fluoride effect on the content of anatase. It can be seen that (1) R increases with increasing the content of anatase, and (2) only if the content of anatase is greater than 40%, can fluoride play a positive role ($R > 1$) on the photocatalytic activity of TiO_2 (Fig. 12B).

3.8. Hydroxyl radicals quenching and detection

It has been proposed that the free •OH radical mediated oxidation pathways are enhanced on F-TiO_2 (Eq. (2)), whereas the hole transfer mediated oxidations are largely inhibited due to the hindered adsorption of substrates on F-TiO_2 (Fig. 10) [12]. To verify whether •OH radicals are involved, the photocatalytic degradation of X3B is carried out in the presence of *tert*-butyl alcohol (TBA), a widely used •OH scavenger ($k = 6 \times 10^8$ M^{-1} s^{-1}) [19]. Fig. 13 shows the effect of TBA (10%, v/v) on the photocatalytic degradation of X3B (pH 3.0) in the suspensions of AT100 and AT0, respectively. The presence of TBA greatly suppressed the

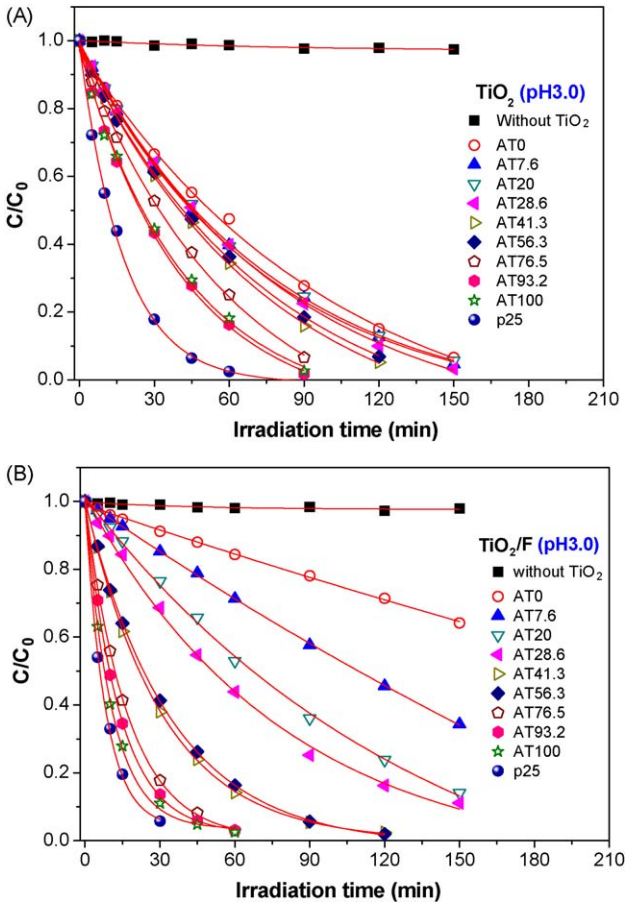

Fig. 11. Photocatalytic degradation of X3B under UV irradiation at pH 3.0 in naked (A) and fluoride modified TiO_2 (B) with different contents of anatase. The concentration of TiO_2 and fluoride are 1.0 g/L and 1.0 mmol/L, respectively.

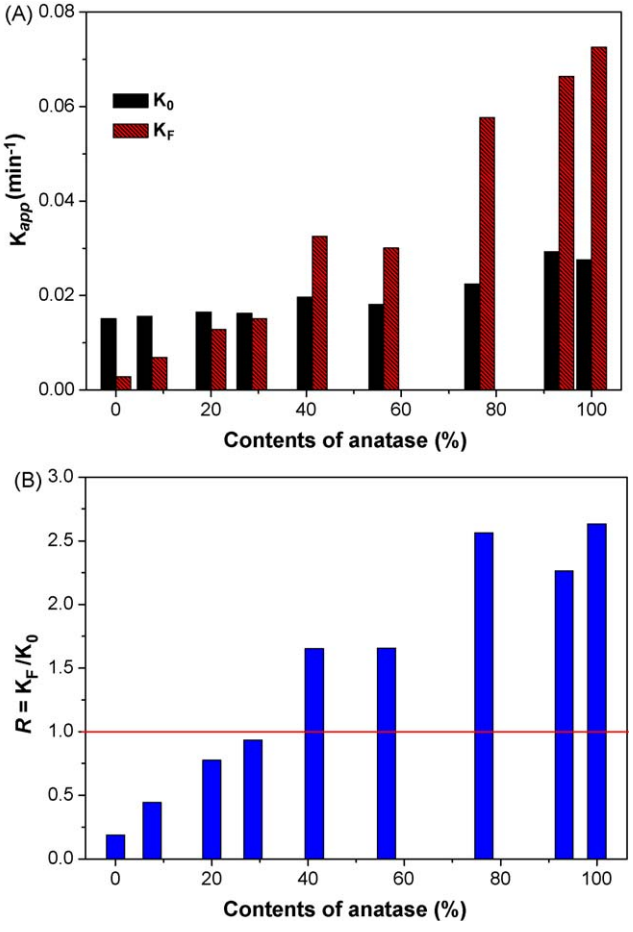

Fig. 12. Degradation rate constants of X3B on TiO_2 samples with different contents of anatase in the absence and presence of NaF (A), and the corresponding ratios of the observed rate constants after and before the addition of fluoride (B).

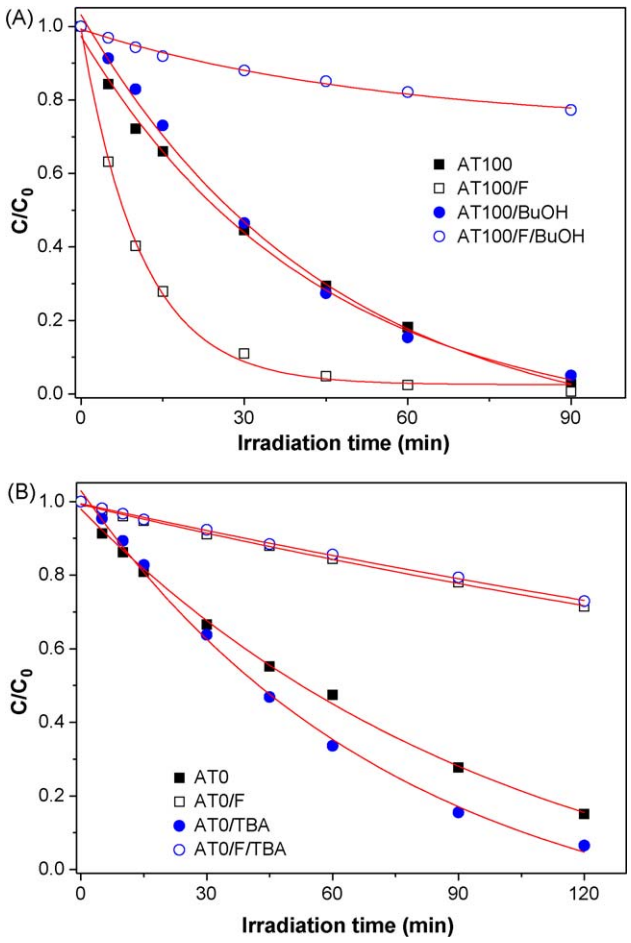

Fig. 13. Effect of TBA (10%, v/v) on the photocatalytic degradation of X3B on AT100 and AT0 in the absence and presence of NaF.

degradation rate of X3B on fluorinated AT100 (rate constant decreases from 0.073 min^{-1} to 0.00276 min^{-1}). However, as for naked AT100, no such inhibitory effect of TBA was observed. The results suggest that the photocatalytic degradation of X3B on naked AT100 is predominately initiated by direct hole transfer, whereas the reaction on fluorinated AT100 is through •OH radicals and valence holes. This explanation is similar to those previous report for the rate enhancement of weakly adsorptive substrate phenol on F-TiO_2 [13,20]. No inhibitory effect of TBA were observed both on the naked and fluorinated AT0. It was found that the relevant rate constants for fluorinated AT0 were 0.00280 and 0.00256 min^{-1} in the absence and presence of TBA, respectively. These results infer that, different from anatase (AT100), little •OH radicals were involved in the photocatalytic degradation of X3B on naked and fluorinated rutile (AT0). This is also confirmed by the •OH radicals detection technique using coumarin as a probe molecule (Scheme 1), which will be shown below.

It should be noted that, as for AT0 sample, the presence of TBA enhances the photocatalytic degradation of X3B (Fig. 13B). One of the possible reasons is that the presence of TBA, an organic solvent, accelerates the desorption of the degraded intermediates of X3B from the surface of TiO_2. Then, more active sites are left for fresh X3B to be degraded. Compared with anatase, rutile TiO_2 shows poorer oxidative ability due to the quicker electron-hole recombination rate (Fig. 7). It infers that the dye, X3B, is only decomposed to some extend, and far to minerize to CO_2 and H_2O in the suspensions of AT0. However, this needs to be studied further.

Recently, it has been proved that several non- or weakly luminescent test molecules, such as terephthalic acid [41,42] and coumarin [30,31,41] produce strongly luminescent compounds with •OH radical. Hence, these molecules can be applied for detection and measurement of •OH radicals. Here coumarin is used to detect the formation of free •OH radicals in fluorinated TiO_2 (AT0, AT100 and p25) at pH3.0. Fig. 14A and B shows the fluorescence spectral changes observed during illumination of the suspensions of fluorinated AT0 and AT100, respectively. It is observed that the fluorescence intensity of photo-generated 7-hydroxycoumarin at 450 nm (excited at 332 nm) increases with irradiation time, and fluorinated AT100 shows more obvious spectral changes of fluorescence intensity than that of AT0. Fig. 14C

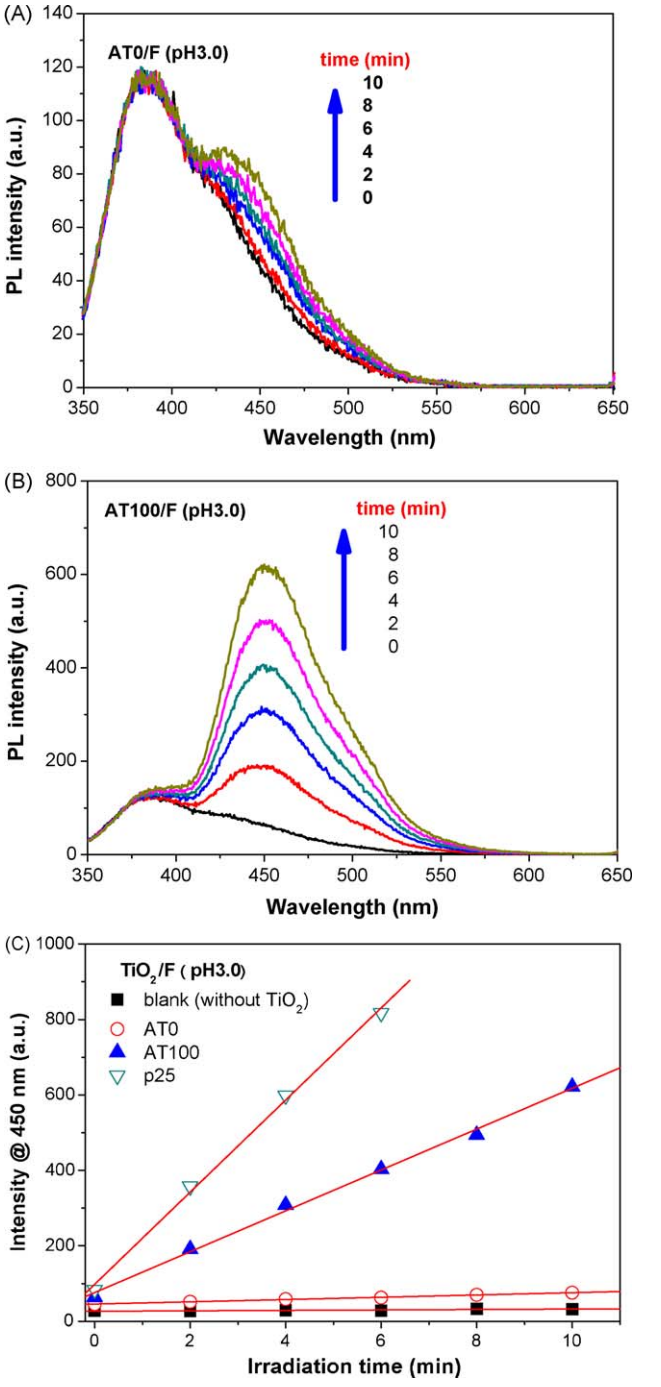

Fig. 14. Fluorescence spectral changes observed during illumination of the suspensions of fluorinated (A) AT0 and (B) AT100, and (C) time dependence of the induced fluorescence intensity @ 450 nm for fluorinated AT0, AT100, p25 and control experiment, respectively.

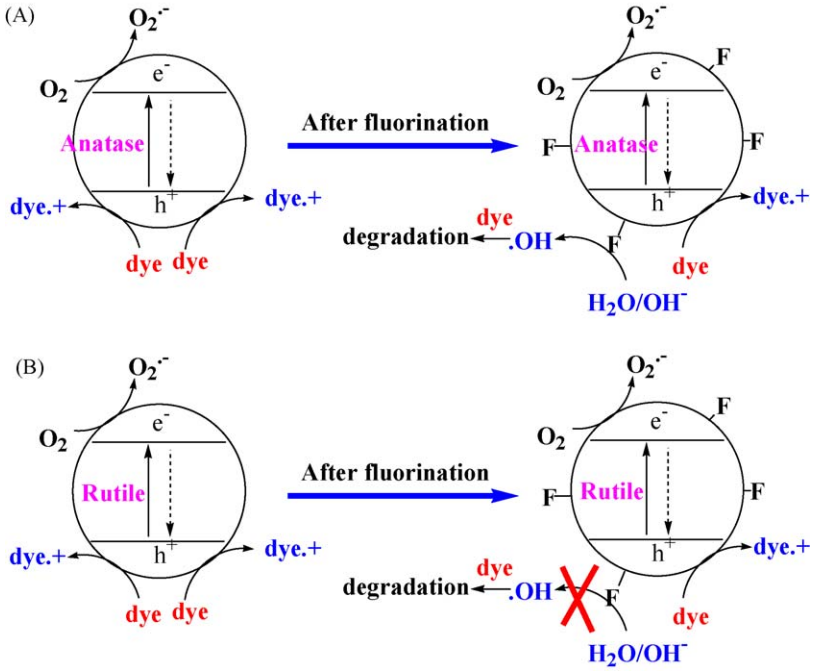

Fig. 15. Schematic diagrams for the photocatalytic degradation pathways of X3B in anatase (A) and rutile (B) TiO_2 in the absence and presence of NaF at pH 3.0.

records the time course of the fluorescence intensity of 7-hydroxycoumarin at 450 nm during the irradiation. It is clearly seen that the fluorescence intensity at 450 nm increases linearly against the irradiation time. This leads to a conclusion that the generation of fluorescent 7-hydroxycoumarin is linearly proportional to illumination time, obeying a pseudo-zero-order reaction rate equation in kinetics. The slopes for the curve of fluorescent intensity *versus* illumination time, which represent the formation rate of free •OH radicals in solution, are measured as 2.996, 54.14 and 122.1 for AT0, AT100 and p25, respectively. Blank experiment (in the absence of TiO_2) gives a slope of 0.5891. Therefore, the formation of free •OH radicals in fluorinated AT0 sample is negligible, which is consistent with the •OH radical quenching experimental results (Fig. 13B). The failure oxidation solvent water to form free •OH radical in fluorinated AT0 (Eq. (2)) may be due to the quick electron-hole recombination rate, which has been characterized by photocurrent response (Fig. 7).

3.9. Reaction models

Comparing the photocatalytic degradation kinetics, photocurrent response, •OH radical quenching and detection, between anatase and rutile TiO_2 in the absence and presence of fluoride provides valuable mechanistic information. Both for anatase and rutile TiO_2, the presence of fluoride suppresses the adsorption of X3B due to the reduction of positive charge of TiO_2 after the surface is occupied by fluoride (Fig. 10). The degradation pathway of X3B transfers from direction holes oxidation to free •OH radicals-mediated oxidation (Eq. (2)).

Although photo-generated holes should have higher oxidation power than •OH radicals, surface fluorination can greatly accelerate the formation of free •OH radicals in solution [17]. Direct hole oxidation can only take place on the surface of TiO_2. However, degradation of organic pollutant by free •OH radicals can be performed in solution homogeneously (Eq. (2)) [12,13,19]. Therefore, it was hypothesized that the relative reactivity of free •OH radical is higher than that of subsurface h_{vb}^+ [19]. Then it is not too hard to understand the positive effect of surface fluorination on the photocatalytic activity of anatase TiO_2 (Fig. 15A).

However, different from anatase TiO_2, little •OH radical is detected in fluorinated rutile TiO_2, ascribed to the failure oxidation of solvent water by hole to form •OH radical (Figs. 13 and 14) due to the quick recombination of photo-generated electron and hole (Fig. 7). The photoluminescence (PL) study (Jung et al.) [43] suggested that the inferior photocatalytic activity of rutile nanoparticles is correlated with the intrinsic recombination of photo-generated electron–hole pairs. It is supposed that electron transfer between photo-generated hole and solvent water to form free •OH radical in fluorinated TiO_2, is the rate determining step. From the viewpoint of dynamics, the short life time of the hole is unfavorable for the oxidation of solvent water, which should be responsible for the failure formation of free •OH radicals in fluorinated rutile TiO_2. Therefore, both in naked and fluorinated rutile TiO_2, holes are the only oxidative species responsible for the degradation of X3B (Fig. 15B). As the direct hole transfer is suppressed due to hindered adsorption of X3B (Fig. 10), fluoride surface modification is sure to be detrimental to the photocatalytic activity of rutile TiO_2 (Fig. 15B).

We have found that fluoride effection depends on the photocatalytic activity of naked anatase TiO_2 [40], and the related study is being in progress. Calcination treatment can influence the crystallinity of the obtained TiO_2 samples, and thus the photocatalytic activity of TiO_2. Therefore, calcination temperature also plays an important role on fluoride effection. Considering that anatase phase is irreversibly converted to the less reactive rutile phase at about 600 °C under normal conditions [37]. 500 °C is selected as the calcined temperature in the present work, to prevent the phase transformation of anatase-to-rutile and to get a more distinct fluoride effection.

It is noted that the dye X3B is quite stable against UV irradiation in solution (Fig. 11). The dye degradation under visible light irradiation ($\lambda \geq 450$ nm) *via* photosensitization pathway is much slower than that under UV irradiation [19,39].

4. Conclusions

Nanocrystalline TiO_2 catalysts for different contents of anatase with similar BET surface areas and crystalline sizes were prepared

by hydrothermal treatment of the solution of $Ti(SO_4)_2$ and/or $TiCl_4$. By simply varying the proportion of $Ti(SO_4)_2$ and $TiCl_4$, TiO_2 powders with different contents of anatase and rutile phases were obtained. Those TiO_2 samples show similar adsorption to fluoride, and the adsorption of X3B increases with increasing the content of anatase. However, for both anatase and rutile TiO_2, the adsorption of X3B is severely suppressed in the presence of fluoride, which could be ascribed to competitive adsorption of fluoride that reduces the positive charges on the catalyst surface. Fluoride effection increases with increasing the content of antase. Only when the content of anatase is higher than 40% in the mixed TiO_2, can fluoride play a positive role on the photocatalytic activity of TiO_2. As for anatase TiO_2, photocatalytic degradation pathway of X3B shifts from direct hole oxidation to free $^{\bullet}OH$ radicals oxidation after surface fluorination. However, direct holes oxidation are the only way for the degradation of X3B in rutile TiO_2, irrespective of the absence and presence of fluoride. Since the various synthetic nanocrystalline TiO_2 catalysts are of similar BET surface areas and crystalline sizes, the difference in crystalline phase should be considered as the most important reason to be responsible for the different effect of fluorination on the photocatalytic activity of anatase and rutile TiO_2. Failure formation of free $^{\bullet}OH$ radicals in rutile TiO_2, due to the quick recombination of photo-generated electron–hole pairs, is responsible for the negative effect of fluoride on the degradation of X3B. This study may provide new insight into design and preparation of advanced photocatalytic materials.

Acknowledgments

This work was supported by the National Natural Science Foundation of China (20977114, 20977115 and 20807057), Natural Science Foundation of Hubei Province (2008CDB265) and China Postdoctoral Science Foundation (20090451086).

References

[1] M.C. Yan, F. Chen, J.L. Zhang, M. Anpo, J. Phys. Chem. B 109 (2005) 8673.
[2] J.G. Yu, S.W. Liu, H.G. Yu, J. Catal. 249 (2007) 59.
[3] W.P. Du, Y.M. Xu, Y.S. Wang, Langmuir 24 (2008) 175.
[4] Y.M. Chen, F. Chen, J.L. Zhang, Appl. Surf. Sci. 255 (2009) 6290.
[5] Y.M. Xu, C.H. Langford, J. Phys. Chem. B 101 (1997) 3115.
[6] J.G. Yu, Y.R. Su, B. Cheng, Adv. Funct. Mater. 17 (2007) 1984.
[7] X.F. Cheng, W.H. Leng, D.P. Liu, Y.M. Xu, J.Q. Zhang, C.N. Cao, J. Phys. Chem. C 112 (2008) 8725.
[8] M.R. Hoffmann, S.T. Martin, W. Choi, D.W. Bahnemann, Chem. Rev. 95 (1995) 69.
[9] J.G. Yu, W.G. Wang, B. Cheng, B.L. Su, J. Phys. Chem. C 113 (2009) 6743.
[10] K.L. Lv, H.S. Zuo, J. Sun, K.J. Deng, S.C. Liu, X.F. Li, D.Y. Wang, J. Hazard. Mater. 161 (2009) 396.
[11] X.F. Li, K.L. Lv, K.J. Deng, J.F. Tang, R. Su, J. Sun, L.Q. Chen, Mater. Sci. Eng. B 158 (2009) 40.
[12] H. Park, W. Choi, J. Phys. Chem. B 108 (2004) 4086.
[13] C. Minero, G. Mariella, V. Maurino, E. Pelizzetti, Langmuir 16 (2000) 2632.
[14] C. Minero, G. Mariella, V. Maurino, D. Vione, E. Pelizzetti, Langmuir 16 (2000) 8964.
[15] A. Janczyk, E. Krakowska, G. Stochel, W. Macyk, J. Am. Chem. Soc. 128 (2006) 15574.
[16] M. Mrowetz, E. Selli, New J. Chem. 30 (2006) 108.
[17] M. Mrowetz, E. Selli, Phys. Chem. Chem. Phys. 7 (2005) 1100.
[18] M.S. Vohra, S. Kim, W. Choi, J. Photochem. Photobiol. A 160 (2003) 55.
[19] K.L. Lv, Y.M. Xu, J. Phys. Chem. B 110 (2006) 6204.
[20] Y.M. Xu, K.L. Lv, Z.G. Xiong, W.H. Leng, W.P. Du, D.L. Liu, X.J. Xue, J. Phys. Chem. C 111 (2007) 19024.
[21] K.L. Lv, C.S. Lu, Chem. Eng. Technol. 31 (2008) 1272.
[22] J.S. Park, W. Choi, Langmuir 20 (2004) 11523.
[23] H. Kim, W. Choi, Appl. Catal. B 69 (2007) 127.
[24] V. Maurino, C. Minero, G. Mariella, E. Pelizzetti, Chem. Commun. 20 (2005) 2627.
[25] H. Cheng, J.M. Ma, Z.G. Zhao, L.M. Qi, Chem. Mater. 7 (1995) 663.
[26] H. Luo, C. Wang, Y. Yan, Chem. Mater. 15 (2003) 3841.
[27] M.M. Wu, J.B. Long, A.H. Huang, Y.J. Luo, Langmuir 15 (1999) 8822.
[28] J.G. Yu, M.H. Zhou, B. Cheng, X.J. Zhao, J. Mol. Catal. A 246 (2006) 176.
[29] M.H. Zhou, J.G. Yu, S.W. Liu, P.C. Zhai, B.B. Huang, Appl. Catal. B 89 (2009) 160.
[30] H. Czili, A. Horvath, Appl. Catal. B 81 (2008) 295.
[31] H.M. Guan, L.H. Zhu, H.H. Zhou, H.Q. Tang, Anal. Chim. Acta 608 (2008) 73.
[32] J. Zhang, M.J. Li, Z.C. Feng, J. Chen, C. Li, J. Phys. Chem. B 110 (2006) 927.
[33] Q.H. Zhang, L. Gao, Langmuir 19 (2003) 967.
[34] S. Kittaka, K. Matsuno, S. Takahara, J. Solid State Chem. 132 (1997) 447.
[35] M.H. Zhou, J.G. Yu, J. Hazard. Mater. 152 (2008) 1229.
[36] P. Periyat, S.C. Pillai, D.E. McCormack, J.C. Colreavy, S.J. Hinder, J. Phys. Chem. C 112 (2008) 7644.
[37] P. Periyat, D.E. McCormack, S.J. Hinder, S.C. Pillai, J. Phys. Chem. C 113 (2009) 3246.
[38] Z.S. Sun, Y.X. Chen, Q. Ke, Y. Yang, J. Yuan, J. Photochem. Photobiol. A 149 (2002) 169.
[39] Y.M. Xu, C.H. Langford, Langmuir 17 (2001) 897.
[40] K.L. Lv, J.G. Yu, K.J. Deng, J. Sun, Y.X. Zhao, D.Y. Du, M. Li, J. Hazard. Mater. 173 (2010) 539.
[41] K. Ishibashi, A. Fujishima, T. Watanabe, K. Hashimoto, Electrochem. Commun. 2 (2000) 207.
[42] Q. Xiao, Z.C. Si, J. Zhang, C. Xiao, X.K. Tan, J. Hazard. Mater. 150 (2008) 62.
[43] H.S. Jung, H. Kim, Electron. Mater. Lett. 5 (2009) 73.